

RNA-binding protein CPEB1 remodels host and viral RNA landscapes

Ranjan Batra^{1-3,10}, Thomas J Stark^{1-4,10}, Elizabeth Clark^{1,4,5}, Jean-Philippe Belzile^{1,5}, Emily C Wheeler¹⁻³, Brian A Yee¹⁻³, Hui Huang¹⁻³, Chelsea Gelboin-Burkhart¹⁻³, Stephanie C Huelga¹⁻³, Stefan Aigner¹⁻³, Brett T Roberts¹⁻³, Tomas J Bos¹⁻³, Shashank Sathe¹⁻³, John Paul Donohue⁶, Frank Rigo⁷, Manuel Ares Jr⁶, Deborah H Spector^{1,4,5} & Gene W Yeo^{1-3,8,9}

Host and virus interactions occurring at the post-transcriptional level are critical for infection but remain poorly understood. Here, we performed comprehensive transcriptome-wide analyses revealing that human cytomegalovirus (HCMV) infection results in widespread alternative splicing (AS), shortening of 3' untranslated regions (3' UTRs) and lengthening of poly(A)-tails in host gene transcripts. We found that the host RNA-binding protein CPEB1 was highly induced after infection, and ectopic expression of CPEB1 in noninfected cells recapitulated infection-related post-transcriptional changes. CPEB1 was also required for poly(A)-tail lengthening of viral RNAs important for productive infection. Strikingly, depletion of CPEB1 reversed infection-related cytopathology and post-transcriptional changes, and decreased productive HCMV titers. Host RNA processing was also altered in herpes simplex virus-2 (HSV-2)-infected cells, thereby indicating that this phenomenon might be a common occurrence during herpesvirus infections. We anticipate that our work may serve as a starting point for therapeutic targeting of host RNA-binding proteins in herpesvirus infections.

Human herpesvirus infections are highly prevalent and substantially affect health worldwide. HCMV, a herpesvirus family member, infects nearly 100% of individuals in the United States by the time they reach adulthood¹, and >5,000 of the infants born with HCMV infections in the United States each year have pervasive developmental deficits. Infection can cause severe neurological defects in newborns and severe disease in immunocompromised individuals²⁻⁴, and it has also been associated with glioblastoma and atherosclerosis⁵⁻⁸. Therapeutic options are limited, and there is currently no vaccine to prevent infection. HCMV infects a variety of cell types, but the interaction and response between viral and host transcriptomes remains largely unclear. In early stages of herpesvirus infection, the cellular environment must be poised for viral replication, and for some herpesviruses, a complete shutdown of host transcription and protein synthesis occurs⁹⁻¹¹. This is not the case for HCMV infections, in which no overall decrease in host mRNA levels occurs¹². An efficient avenue for rapid alteration of the host cellular environment is the modulation of cellular RNA processing. Host RNA-regulatory factors capable of such wide-ranging changes may be responsible for progressive HCMV lytic infection, and although viral gene expression and splicing have been studied^{13,14}, the changes in host RNA processing during HCMV infection are largely unexplored.

Nuclear RNA-processing functions such as alternative cleavage and polyadenylation (APA) are responsible for generating the functional mammalian transcriptome necessary for tissue development and maintenance¹⁵⁻¹⁷. The importance of proper control of AS and APA is highlighted by a number of human diseases that occur as a result of defects in these processes¹⁷⁻²⁰. For example, global AS defects that lead to disease manifestations have been associated with myotonic dystrophy and spinal muscular atrophy¹⁵, and global changes in APA have also been observed in myotonic dystrophy, oculopharyngeal muscular dystrophy and amyotrophic lateral sclerosis^{15,17,21}. In the cytoplasm, the cytoplasmic polyadenylation (cPA) machinery targets RNAs containing a short poly(A) tail²². Cytoplasmic polyadenylation element binding protein 1 (CPEB1) recognizes cytoplasmic polyadenylation elements (CPEs) in RNA substrates and leads to the recruitment of the poly(A) polymerase (PAP) GLD2, which elongates the poly(A) tail²². Changes in poly(A)-tail length alter the translation of certain transcripts, and increased PAP activity has been linked to poor prognosis in some cancers²³. The recent availability of techniques such as poly(A)-tail length profiling by sequencing (PAL-seq)²⁴ and genome-wide determination of poly(A)-tail length and 3'-end modifications (TAIL-seq)²⁵ has enabled genome-wide measurements of poly(A)-tail lengths.

¹Department of Cellular and Molecular Medicine, University of California at San Diego, La Jolla, California, USA. ²Stem Cell Program, University of California at San Diego, La Jolla, California, USA. ³Institute for Genomic Medicine, University of California at San Diego, La Jolla, California, USA. ⁴Division of Biological Sciences, University of California at San Diego, La Jolla, California, USA. ⁵Skaggs School of Pharmacy and Pharmaceutical Sciences, University of California at San Diego, La Jolla, California, USA. ⁶RNA Center, Department of Molecular, Cell and Developmental Biology, Sinsheimer Labs, University of California, Santa Cruz, Santa Cruz, California, USA. ⁷Ionis Pharmaceuticals, Carlsbad, California, USA. ⁸Molecular Engineering Laboratory, A*STAR, Singapore. ⁹Department of Physiology, Yong Loo Lin School of Medicine, National University of Singapore, Singapore. ¹⁰These authors contributed equally to this work. Correspondence should be addressed to G.W.Y. (geneyeo@ucsd.edu).

Received 1 August; accepted 22 September; published online 24 October 2016; doi:10.1038/nsmb.3310

However, transcriptome-wide changes in poly(A)-tail lengths have not been determined in human disease and viral infections.

RNA-binding proteins (RBPs) are responsible for regulating RNA processing and shaping the RNA landscapes in cells, and they consequently determine cellular fates in differentiation and disease. Families of RBPs such as muscleblind-like (MBNL), NOVA, RBFox and heterogeneous nuclear ribonucleoproteins (hnRNPs) have been shown to control both AS and APA^{17,19,26–29}. However, the involvement of RBPs in the modulation of host or viral transcriptomes during virus infections remains poorly understood. In this study, transcriptome-wide analyses revealed that HCMV infection leads to widespread host and viral gene expression and RNA-processing changes. Unexpectedly, we discovered that the RBP CPEB1 is upregulated during HCMV infection. Exogenous expression of CPEB1 in the absence of HCMV infection recapitulated infection-related host AS and APA patterns. Additionally, depletion of CPEB1 during HCMV infection led to the reversal of a large fraction of infection-related host AS, APA and cPA changes. Strikingly, decreased CPEB1 led to shortened viral poly(A)-tail lengths in CPEB1-bound substrates, decreased protein levels of late viral proteins and decreased productive viral titers. Our results demonstrate that CPEB1 is required for modulating host and viral transcripts necessary for full-blown lytic HCMV infection.

RESULTS

Host RNA processing is extensively altered in HCMV infection

To assess mRNA expression patterns of host and HCMV genes, we generated poly(A)⁺ RNA-seq libraries from primary human foreskin fibroblasts (HFFs), human aortic endothelial cells (ECs) and human embryonic stem (ES) cell-derived neural progenitor cells (NPCs) at both 48 and 96 h postinfection (hpi) with the clinical HCMV isolate TB40E (multiplicity of infection (MOI) of 5; **Supplementary Fig. 1a**). These are commonly infected cell types that support varying degrees of viral infection³⁰. Indeed, although viral gene expression correlated with infection time points in HFF, EC and NPC cells (**Supplementary Fig. 1b**; based on annotated HCMV open reading frames), we observed marked expression changes in viral genes in HFFs and ECs at 96 hpi, but not in NPCs (**Supplementary Fig. 1c,d** and **Supplementary Data Set 1**). This finding was consistent with previous observations of nonprogressive infection in this NPC model³⁰. Nonetheless, HCMV mRNA expression was similar in the three cell lines at early times during the infection (**Supplementary Fig. 1b**).

Next, we evaluated alterations in host-cell RNA-processing pathways as a result of HCMV infection. Using splicing-sensitive Affymetrix microarrays, we found >2,000 significantly altered host RNA splicing events (**Fig. 1a,b** and **Supplementary Data Set 2**) in HCMV-infected HFFs and NPCs²⁸. Although NPCs exhibited fewer AS changes, half of the NPC alternative-cassette events overlapped with changes in HFFs (**Fig. 1a** and **Supplementary Data Set 2**), thus demonstrating that a similar AS program is established by HCMV infection. To study APA changes in host transcripts, we used the mixture of isoforms (MISO) algorithm²⁷ to survey tandem 3'-UTR events and alternative 3'-terminal exons detected in the RNA-seq data. Interestingly, the majority of these events resulted in shortened 3' UTRs after infection in the three cell types (**Fig. 1a** and **Supplementary Data Set 3**). We validated both AS (exons in *USPL1*, *CAST* and *MYO18A* transcripts in **Fig. 1c**) and APA (3' UTRs in *PCGF3*, *ANKH* and *MARCH6* transcripts in **Fig. 1d,e** and **Supplementary Fig. 2a,b**) events that were specific to either the infected NPCs or HFFs and ECs. For APA, the lengths of affected transcripts were generally shortened (**Fig. 1f**) by 1–5 kb by 96 hpi (**Supplementary Fig. 2c**). We also generated RNA-seq data from HFFs infected with HSV-2 at 8 hpi and analyzed APA with the MISO algorithm (**Supplementary**

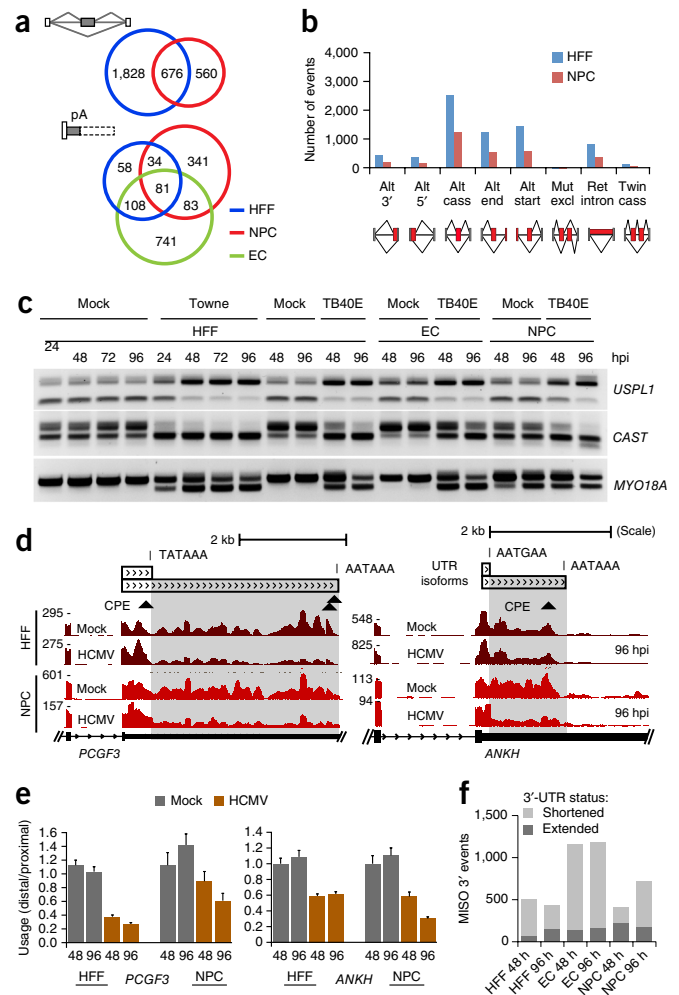


Figure 1 Host RNA-processing patterns are altered during HCMV infection. (a) Overlap of alternative cassette-exon splicing events (top) and APA events (bottom) among infected HFFs, NPCs and ECs ($n = 1$ experiment for each condition for each cell type; MOI 5). (b) Numbers and types of infection-altered splicing events in NPCs and HFFs, detected by splicing-sensitive microarrays of Towne-infected HFFs at 72 hpi and TB40E-infected NPCs at 96 hpi. Alt, alternative; cass, cassette; mut excl, mutually exclusive; ret, retained. (c) RT-PCR validation of alternative-cassette events in mock- and HCMV-infected HFFs, NPCs and ECs (3/3 selected events were validated). (d) RNA-seq coverage of *PCGF3* and *ANKH*, showing 3'-UTR shortening in HCMV-infected NPCs (96 hpi) and HFFs. Predicted canonical CPEB1-recognition sites (CPEs, specifically (U)UUUU(U) or UUUU(U)), are indicated by triangles below the 3' UTRs. (e) qRT-PCR validation of decreased distal 3'-UTR usage in *PCGF3* and *ANKH* mRNA transcripts (4/5 targets selected were validated). Data are shown as mean \pm s.e.m. ($n = 3$ qRT-PCR reactions). (f) Identification of altered 3'-UTR isoform usage determined by the MISO algorithm in the indicated HCMV viral infection conditions. Source Data for **e** and **f** are available online.

Data Set 3e). We found 278 altered events (173 (~62%) 3'-UTR shortening events, **Supplementary Fig. 2d**) out of which 51 events (18%) were common with HCMV APA events (**Supplementary Fig. 2d**, right) in host transcripts including *ANKH* and *PCGF3* (**Supplementary Fig. 2e,f**). We also found AS changes in transcripts such as *PICALM* (**Supplementary Fig. 2g**). However, we did not find APA changes in T cells infected with the RNA virus HIV-1 (**Supplementary Fig. 2d**). We concluded that AS and APA in host RNA transcripts are dramatically altered by the herpesvirus family members HCMV and HSV-2.

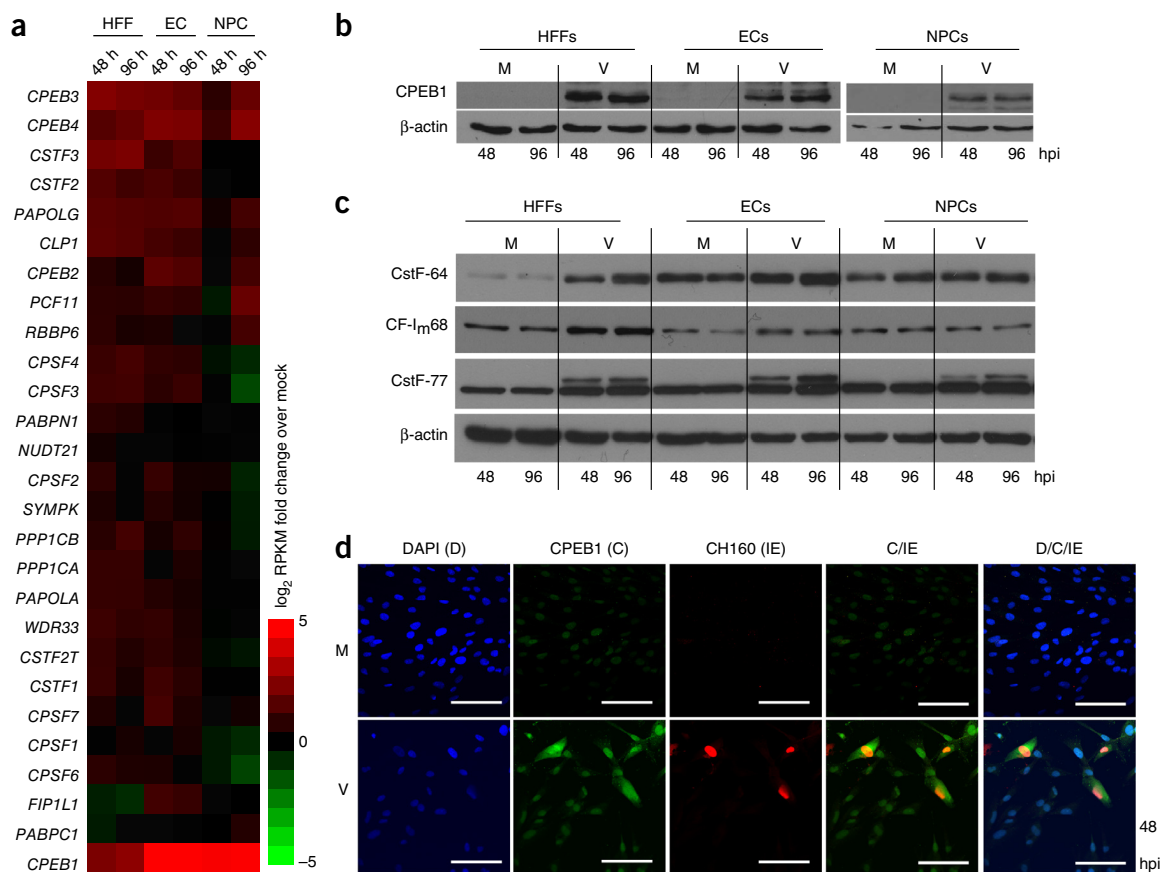


Figure 2 RNA-binding protein CPEB1 is upregulated in HCMV-infected HFFs, ECs and NPCs. **(a)** Heat map of fold change (\log_2) for host 3'-end-processing factors calculated from ratios of reads per kilobase transcript per million mapped reads (RPKM) (normalized to mock infection, MOI 5). Red, upregulated; green, downregulated. **(b)** Immunoblot analysis of CPEB1 upregulation after HCMV TB40E infection (V; MOI 5) compared with mock-infected (M) conditions across three cell types. **(c)** Immunoblot analysis of host core 3'-end-processing factors. β -actin is a loading control. Uncropped blots are shown in **Supplementary Data Set 10**. **(d)** Immunofluorescence of HCMV immediate early (IE) protein CH160 (red) and CPEB1 (C, green) with DAPI nuclear stain (D) in HFFs at 48 hpi (MOI 0.5). Scale bars, 100 μ m.

CPEB1 is consistently upregulated during HCMV infection

The shortening of 3' UTRs among the different cell types suggested the involvement of one or more common RNA-regulatory factors. We evaluated the mRNA abundance (by RNA-seq) of genes during HCMV infection. (**Supplementary Fig. 3** and **Supplementary Data Set 4**), focusing on host RBPs known to regulate APA (**Fig. 2a** and **Supplementary Data Set 4**). Unexpectedly, CPEB1 emerged as the most dramatically and consistently upregulated RBP in all cell types at the mRNA (six-fold in HFFs and over 30-fold in both ECs and NPCs, by 96 hpi) and protein levels during HCMV infection (**Fig. 2b**, **Supplementary Fig. 3d–f** and **Supplementary Data Set 3e**). Protein levels of most of the known mediators of 3'-end formation (including the CstF-64, CstF-77, CF-Im68, CPSF160 and CPSF100 proteins), HNRNP family members (HNRNPH, HNRNPM and HNRNPU) and other CPEB family members were not consistently altered across cell types (**Fig. 2c** and **Supplementary Figs. 3f** and **4a–c**). Interestingly, there was an induction of a longer CstF-77 isoform in all three cell types (**Fig. 2c**), but, according to a previous report, the longer isoform is not associated with 3'-UTR shortening³¹. We observed upregulation of the CstF-64 protein in infected HFFs (**Fig. 2c**), but this upregulation did not affect candidate 3'-UTR shortening events in HFFs (**Supplementary Fig. 4d,e**). To demonstrate specificity for HCMV infection, we treated cells with UV-inactivated HCMV or interferon gamma (IFN- γ), neither of which induced CPEB1 upregulation

(**Supplementary Fig. 4f**) or caused HCMV-related AS in the *SPAG9* and *ITGA6* transcripts (**Supplementary Fig. 4g**). At the subcellular level, CPEB1 upregulation was observed in the infected cells (MOI 0.5) marked with the major immediate early viral proteins (IE1 and IE2; CH160 antibody) at 48 hpi, as detected by immunofluorescence (**Fig. 2d**), and CPEB1 was present in both the nuclei and cytoplasm of HCMV-infected cells. Thus, we concluded that CPEB1 is consistently and robustly upregulated after infection in all three cell types.

CPEB1 expression causes changes reminiscent of HCMV infection

To evaluate whether CPEB1 is indeed responsible for the RNA-processing changes observed during HCMV infection, we ectopically expressed the full-length isoform of CPEB1 in noninfected HFFs (**Fig. 3a**) and subjected the cells to RNA-seq analysis. Strikingly, CPEB1 overexpression (OE) in uninfected cells caused a substantial shift toward utilization of proximal poly(A) sites in transcripts affected during infection (*SYNRG* in **Fig. 3b,c**). Consensus UUUUUUAU sequences (CPE) in proximity to a polyadenylation signal (PAS) are known to recruit CPEB1 to 3'-UTR regions²². Although it remains unknown whether these sequence elements alone are sufficient for the recently proposed role of CPEB1 in RNA processing³², enrichment in these elements has been reported for affected transcripts in regions surrounding alternative cleavage sites. Indeed, we found that ~50% of isoforms that shortened during infection exhibited

CPE-PAS co-occurrences surrounding the proximal 3' ends (250 nt), a value two-fold above that of the isoforms that remained unchanged during infection (Fig. 3d). Additionally, genome-wide comparisons showed that 27% (128/473; Fig. 3e and Supplementary Data Set 3) of the APA changes (detected by RNA-seq) and 43% (276/645, Fig. 3f and Supplementary Data Set 5) of the AS changes (detected by splicing-sensitive microarrays) that were consistent between infected HFFs and NPCs also occurred in CPEB1 OE HFFs without infection. Notably, CPEB1 OE, but not CSTF-77 OE, caused similar AS changes in *MYO18A* and *SPAG9* that resembled changes after HCMV infection yet caused no changes in *USPL1* (Fig. 3g). Therefore, we concluded that CPEB1 is responsible for a large fraction of the RNA-processing changes during HCMV infection in HFFs.

CPEB1 loss reverses HCMV-infection-related RNA changes

The upregulation of CPEB1 and alterations in the host RNA-processing program may be important in establishing the full HCMV lytic infection or may be a downstream effect of the infection itself. To examine these possibilities, we performed RNA-interference-mediated knock-down (KD) of CPEB1 in HFFs 24 h before infection (MOI 3) by using different short interfering RNAs (siRNAs) and achieved >80–90% CPEB1 depletion without decreasing cell viability (Supplementary Fig. 4h,i). To determine the contribution of CPEB1 to RNA-processing changes during HCMV infection of HFFs and to compare the transcriptomes of HCMV-infected and CPEB1-overexpressing HFFs, we performed RNA-seq in mock- and HCMV-infected cells treated with nontargeting (NT) control siRNA and CPEB1-targeting siRNA at 48 hpi, and in HFFs overexpressing GFP (GFP OE) and CPEB1 (CPEB1 OE1 and CPEB1 OE2). Hierarchical clustering of AS changes on the basis of exons altered during HCMV infection demonstrated that HCMV-infected HFFs depleted of CPEB1 (siCPEB1 cells) were similar to mock-infected cells. Notably, uninfected HFFs overexpressing CPEB1 clustered closer to HCMV-infected HFFs (Fig. 4a). Furthermore, 41% (472 of 1,150) of the AS changes established during HCMV infection were either partially or completely reversed after CPEB1 depletion (false discovery rate (FDR) <0.05; Fig. 4a and Supplementary Data Set 6). The partial reversion of AS patterns was probably the result of incomplete KD of CPEB1 or the contribution of other RBPs to the regulation of these events. Evaluation of individual AS events in the transcripts *ITGA6*, *SPAG9* (Fig. 4b,c), *TTC7A* and *MYO18A* (Fig. 4c) with RNA-seq and RT-PCR assays confirmed reversion after CPEB1 depletion during virus infection. Thus, CPEB1 KD reverses HCMV-infection-related AS.

Global APA analysis primarily showed 3'-UTR shortening during infection (Supplementary Fig. 5a) and with CPEB1 overexpression (Supplementary Fig. 5b), and there was a significant overlap in the observed APA changes (Supplementary Fig. 5c). In contrast, we observed 3'-UTR lengthening after CPEB1 depletion in infected cells (Fig. 5a, Supplementary Fig. 5d,e and Supplementary Data Set 3). 196 (of 473; 41%) APA changes in HCMV infection were either partially or completely reversed after CPEB1 KD (Fig. 5a and Supplementary Fig. 5f). *SYNRG* and *ANKH* transcripts that exhibited 3'-UTR shortening during infection maintained their longer 3' UTRs in infected cells after CPEB1 KD (Fig. 5b,c), and *PCGF3* and *ANKH* transcripts showed 3'-UTR shortening in CPEB1 OE HFFs (Supplementary Fig. 5g). Importantly, depletion of CSTF64, a factor known to affect 3' cleavage and polyadenylation of precursor mRNAs did not have this effect (Supplementary Fig. 4e). Interestingly, gene ontology (GO) analysis with Database for Annotation, Visualization and Integrated Discovery (DAVID)³³ and Search Tool for Recurring Instances of Neighboring Genes (STRING)³⁴ of genes with APA

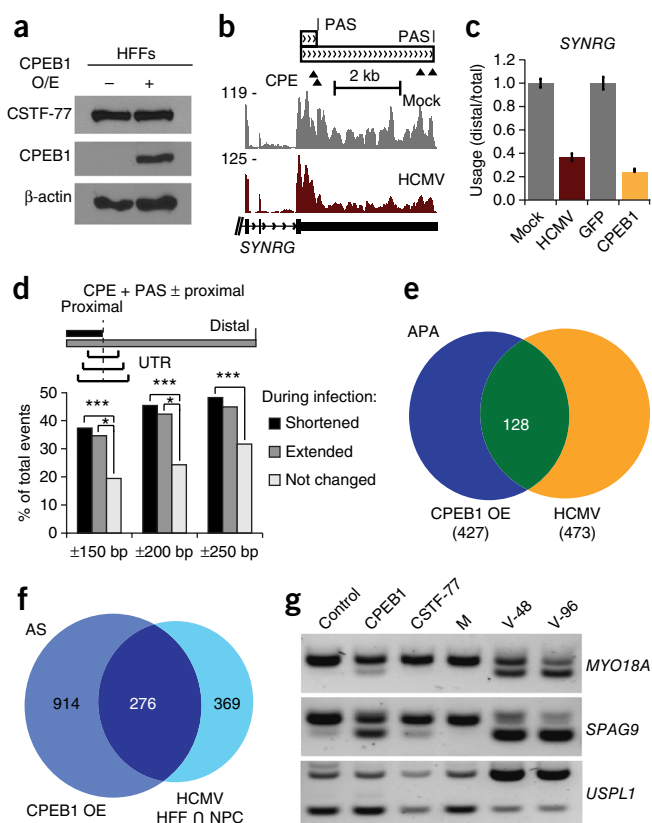


Figure 3 Exogenous CPEB1 expression causes RNA-processing changes reminiscent of HCMV infection. **(a)** Immunoblot of lentivirus-mediated CPEB1 overexpression (OE) in HFFs at 5 d post-transduction. CSTF-77 is shown as a 3'-end-processing-factor control. Uncropped blots are shown in Supplementary Data Set 10. **(b)** RNA-seq coverage of the 3' UTR of *SYNRG* during HCMV and mock infection of HFFs ($n = 1$ RNA-seq experiment per condition). **(c)** qRT-PCR analysis of distal 3'-UTR usage or proximal shift in *SYNRG* after lentivirus-mediated CPEB1 OE (compared with GFP OE as a control). Data are shown as mean \pm s.e.m. ($n = 3$ qRT-PCR reactions). **(d)** Global analysis of the presence of both a canonical CPE ((U)UUUUU or UUUUUAU) on either side and a PAS (AAUAAA or AUUAAA) upstream of RNA-seq-defined 3'-proximal termination sites in increments of 150, 200 and 250 nt. 249 3'-UTR shortening events, 78 lengthening events and 638 control events were considered, and chi-square tests were performed to evaluate significance. *** $P < 0.0001$; * $P < 0.01$. **(e)** Venn diagram showing overlap between APA changes in CPEB1 OE and HCMV-infected HFFs, determined from RNA-seq data ($n = 1$ RNA-seq experiment per condition). **(f)** Venn diagram showing overlap of AS changes in CPEB1 OE and HCMV-infected HFFs and NPCs, measured by splicing-sensitive microarrays ($n = 1$ experiment per condition per cell type). **(g)** RT-PCR analysis of alternatively spliced cassette exons in *MYO18A*, *SPAG9* and *USPL1* mRNA transcripts after OE of GFP (control), CPEB1 or CSTF-77, compared with HCMV (V-) infected HFFs at 48 (V-48) and 96 hpi (V-96). Source data for **c** and **d** are available online.

changes (Supplementary Data Set 7) showed an enrichment in the GO terms 'extracellular exosome' ($P = 7.61 \times 10^{-14}$) and 'Golgi apparatus' ($P = 1.3 \times 10^{-7}$) in HCMV-infected HFFs. These categories were further enriched in siCPEB1 cells (reversal or lengthening events; $P = 2.87 \times 10^{-17}$ and 2.36×10^{-9}) and CPEB1 OE (shortening events, $P = 5.7 \times 10^{-18}$ and 1.5×10^{-8}) altered events (Fig. 5d and Supplementary Fig. 5h). We concluded that CPEB1 KD reverses HCMV-infection-related 3'-UTR shortening.

Because cytoplasmic CPEB1 levels are also higher in HCMV-infected HFFs²², we reasoned that CPEB1 might also modulate the

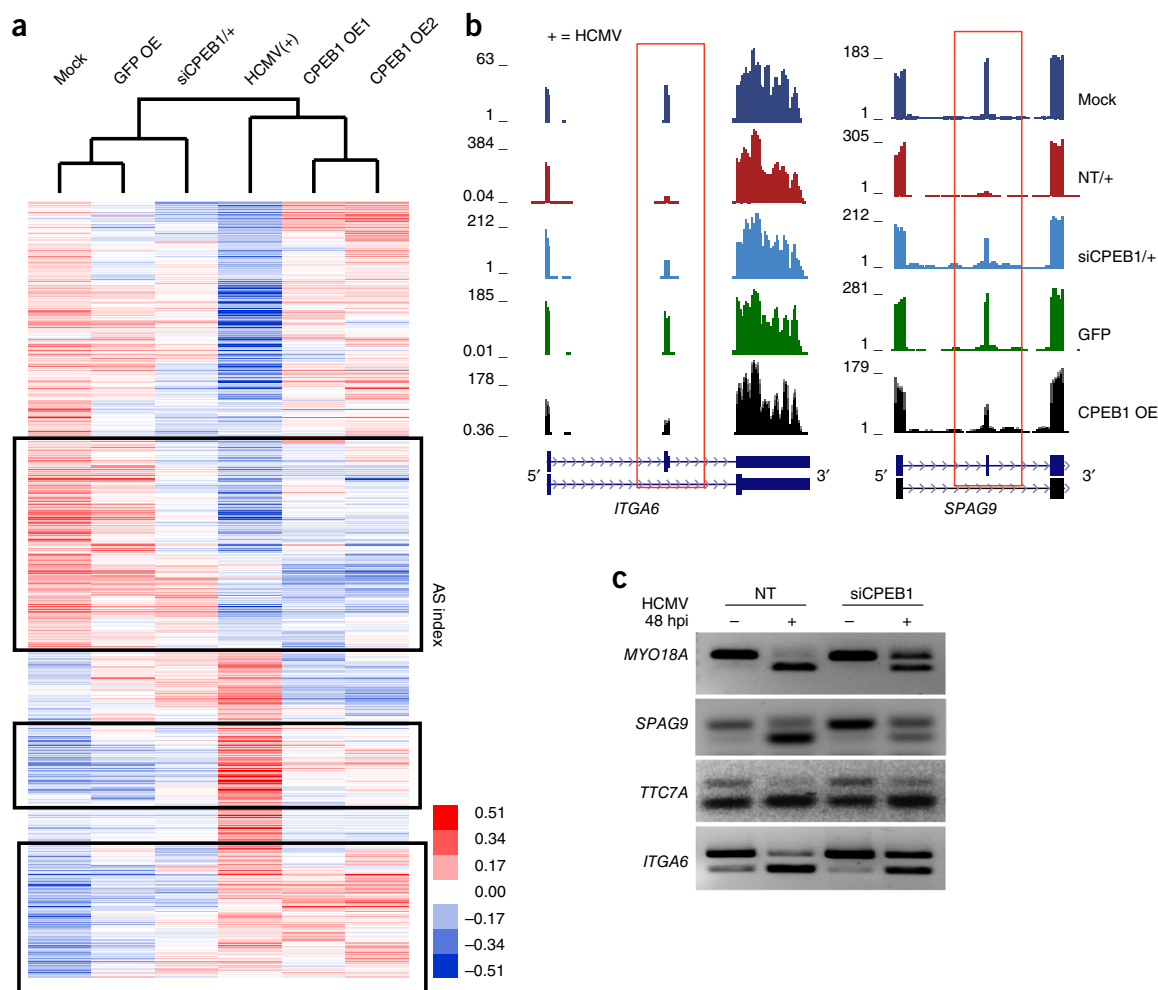


Figure 4 Genome-wide host AS remodeling in HCMV infection is replicated by CPEB1 overexpression and corrected by CPEB1 depletion.

(a) Hierarchical clustering of alternatively spliced exon indices (as a measure of exon inclusion by RNA-seq in HFFs). Boxed regions highlight a reversal of HCMV-infection-related AS (MOI 3). The color bar shows the scale of exon inclusion (positive values) and exclusion (negative values) relative to the mean splicing-index values, in a comparison across samples. 472 exons showed reversal, as reported in **Supplementary Data Set 6** (FDR <0.05, ΔI (a measure of change in exon inclusion) >0.1). HCMV-infected cells are indicated by +. For RNA-seq, $n = 1$ experiment each for mock-infected NT siRNA, HCMV-infected NT siRNA, HCMV-infected siCPEB1, and GFP OE samples; $n = 2$ experiments for CPEB1 OE samples. (b) RNA-seq coverage of AS exons (boxed) in *ITGA6* and *SPAG9* in all conditions in HFF cells. (c) RT-PCR analysis of AS cassette exons (4/4 selected and validated) of *MYO18A*, *SPAG9*, *TTC7A* and *ITGA6* in either mock (-) or HCMV (+)-infected cells treated with either NT or CPEB1 siRNA.

poly(A)-tail lengths of transcripts of both host and viral genes. We performed transcriptome-wide poly(A)-tail length analysis with TAIL-seq²⁵ (**Fig. 5e** and **Supplementary Fig. 6a**), which revealed that the median poly(A)-tail lengths of host transcripts were increased during HCMV infection (**Fig. 5e**). Critically, CPEB1 depletion decreased the median tail lengths to the levels observed after mock infection (**Fig. 5e,f**). GO analysis of host genes whose transcripts had shortened poly(A) tails after CPEB1 depletion showed enrichment ($P = 6 \times 10^{-21}$) in the ‘membrane-enclosed lumen’ category (**Supplementary Data Set 8** and **Supplementary Fig. 6b**). We concluded that CPEB1 depletion during HCMV infection reverses a large fraction of infection-induced RNA-processing changes, including host poly(A)-tail lengths.

CPEB1 depletion shortens poly(A) tails in HCMV transcripts

TAIL-seq analysis of HCMV transcripts in infected (+) and siCPEB1 (+) HFFs showed a decrease in median poly(A)-tail lengths after CPEB1 depletion (**Fig. 6a**). For example, the HCMV transcript

UL18, an MHC I class homolog that participates in evasion of the host immune system³⁵, showed the largest decrease in mean and median poly(A)-tail length (**Fig. 6b** and **Supplementary Data Set 8**). Poly(A)-tail length in the *UL83–UL82* bicistronic transcript was also decreased after CPEB1 depletion, whereas *UL54* did not show a significant change (Mann–Whitney U test; $P = 0.06$; **Fig. 6b**). We performed cross-linking and immunoprecipitation coupled with qRT-PCR (CLIP-PCR) to evaluate whether CPEB1 directly binds to viral transcripts. Indeed, we observed highly increased CPEB1 binding to the *UL99* transcript, which had statistically significant differences in poly(A)-tail length (**Fig. 6b** and **Supplementary Data Set 8**) after CPEB1 depletion, relative to binding of the unrelated RBP fragile X mental-retardation protein (**Fig. 6c**). CPEB1 binding to *UL83* and *UL55* transcripts was also increased three-fold and five-fold over the control, respectively (**Fig. 6c**). *UL55* bound by CPEB1 was not supported by sufficient TAIL-seq reads for poly(A)-tail length detection (**Supplementary Data Set 8**). To assess whether changes in viral protein levels also accompanied alterations in poly(A)-tail length, we performed immunoblot analysis

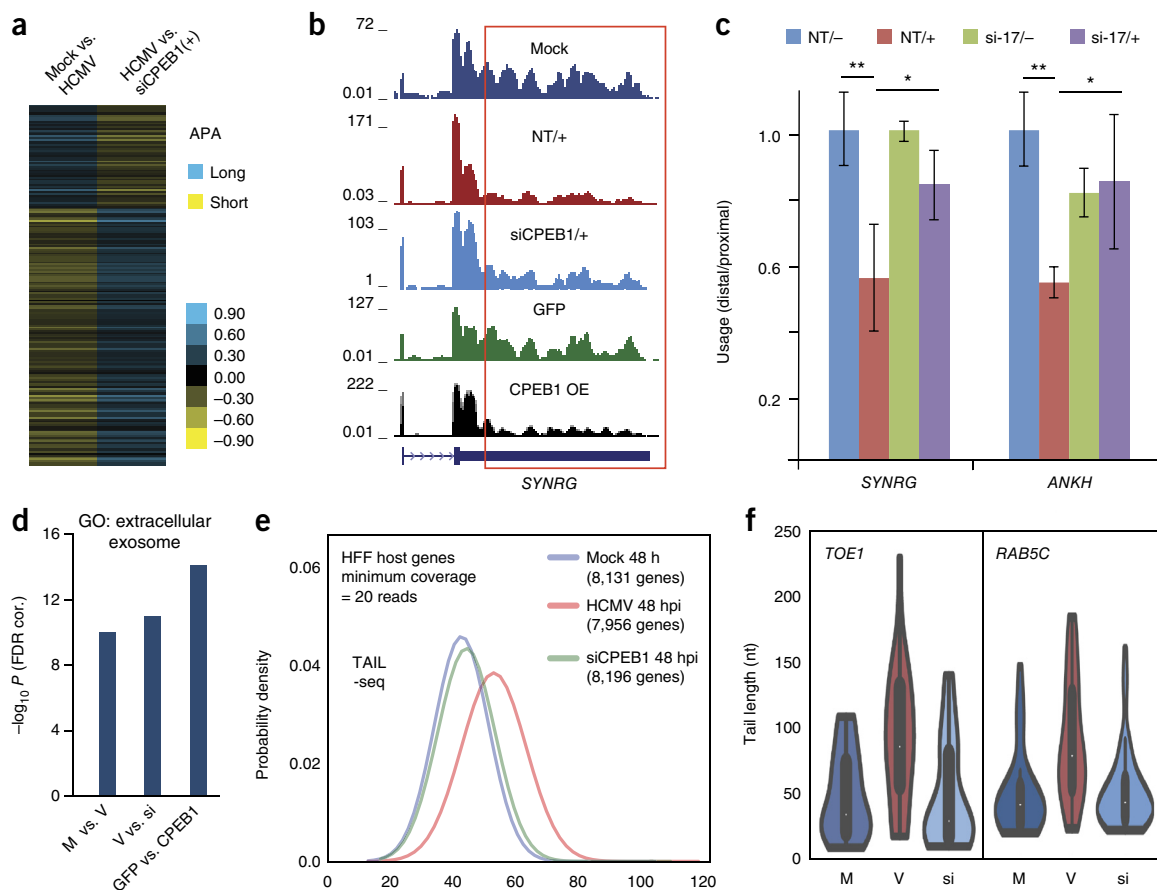


Figure 5 HCMV-infection-related host genome-wide 3'-UTR shortening and poly(A)-tail lengthening in HCMV infection is reversed by CPEB1 depletion. (a) Heat map showing 3'-UTR shortening (yellow) and lengthening (blue) in mock-infected versus HCMV-infected and HCMV-infected versus siCPEB1 cells for 196 transcripts (Bayes factor >10,000) common between two RNA-seq data sets ($n = 1$ RNA-seq experiment per condition). (b) RNA-seq coverage of the *SYNRG* 3' UTR under all conditions in HFF cells. HCMV-infected cells are indicated by +. (c) qRT-PCR analysis of distal 3'-UTR usage in *SYNRG* and *ANKH* transcripts in either mock (-) or HCMV (+)-infected cells treated with either NT or CPEB1 siRNA (si-17). Error bars, s.d. among replicates ($n = 3$ qRT-PCR reactions). ** $P < 0.005$; * $P < 0.05$ by one-tailed Student's t test with unequal variances. (d) DAVID gene ontology (GO) analysis, showing progressive enrichment in the extracellular exosome category in mock (M) versus HCMV (V); HCMV versus siCPEB1 (si) (+HCMV); and GFP OE versus CPEB1 OE. Cor, correction. (e) Median poly(A)-tail lengths determined by TAIL-seq ($n = 2$ MiSeq runs per condition, data sets from two runs were pooled for final analysis) in HCMV-infected HFFs (MOI 3) versus mock-infected controls and siCPEB1 HFFs (+HCMV). (f) Violin plots showing distribution of poly(A)-tail lengths for *TOE1* and *RAB5C* transcripts (mock-infected (M) versus infected (V) $P < 0.0025$ and $P < 5 \times 10^{-5}$, respectively; infected versus siCPEB1 (si) $P < 0.0015$ and $P < 2 \times 10^{-6}$ by one-sided Mann-Whitney U test, respectively). Numbers of transcripts (n) are as follows for *TOE1* and *RAB5C*, respectively: M, $n = 22, 28$; V, $n = 25, 43$; si, $n = 33, 63$. Source data for c–e are available online.

of viral proteins. Our results revealed that the level of the late viral protein pp28 (encoded by *UL99*) was consistently lower in the CPEB1-depleted HCMV-infected (+) HFFs, whereas the immediate early proteins IE-72 and IE-86 showed no changes (Fig. 6d).

CPEB1 is necessary for productive HCMV infection

To evaluate the cellular effects of CPEB1 depletion on viral infection, we analyzed siCPEB1, HCMV-infected HFFs. The morphology of the infected HFFs (MOI 0.5) with CPEB1 depletion at 48 hpi exhibited a dramatic visible rescue of the cytopathic effects normally observed after infection, as compared with the effects in infected cells treated with NT control siRNA (Fig. 7a). The infected siCPEB1 HFFs maintained fibroblast-like characteristics similar to those of healthy mock-infected cells. Productive HCMV titers established with a plaque-forming assay showed an approximately ten-fold decrease in siCPEB1 HFFs compared with NT-siRNA-transfected HFFs at 96 h (Fig. 7b). The titers recovered, at least partially, by 144 hpi. Notably, overexpression of the *UL99*-encoded protein pp28 alone in

siCPEB1-treated, HCMV-infected cells did not result in infection-related morphology at 48 hpi, whereas lentivirus-mediated expression of a codon-optimized CPEB1-GFP fusion that was insensitive to the CPEB1-specific siRNA recapitulated the infection-related morphology in cells (Supplementary Fig. 6c). Indeed, another late protein, *UL83*-encoded pp65, was also decreased after CPEB1 depletion (Fig. 7c). As an orthogonal approach to deplete CPEB1, we used uniformly modified 2'-O-methoxyethyl antisense oligonucleotides (ASOs) with a phosphorothioate backbone against exon 5 in *CPEB1* (Supplementary Data Set 9 and Supplementary Fig. 6d,e). ASO-mediated depletion of CPEB1 decreased the viral pp28 protein levels and rescued the AS changes in *SPAG9* (Supplementary Fig. 6f). Therefore, we concluded that CPEB1 is necessary for shaping the RNA landscapes of host and HCMV genes and supporting productive infection (Fig. 7d).

DISCUSSION

Human gene transcripts are subject to post-transcriptional regulation at the level of AS, APA and poly(A)-tail length during



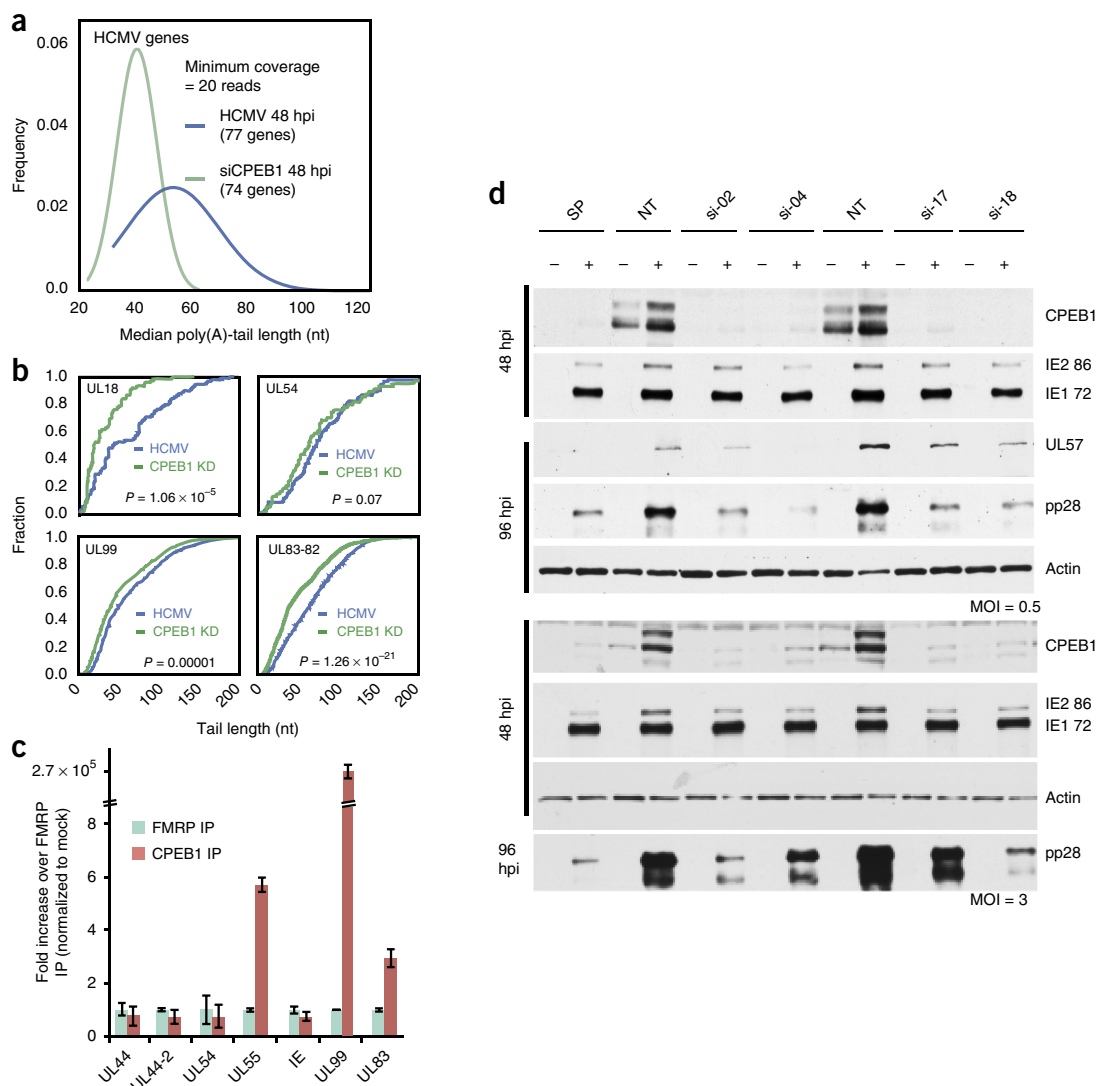


Figure 6 CPEB1 depletion by siRNA results in shortened poly(A)-tail lengths and decreased protein levels for HCMV late genes. **(a)** TAIL-seq distributions ($n = 2$ MiSeq runs per condition, data sets from two runs were pooled for final analysis) of median poly(A)-tail lengths of viral transcripts in HCMV-infected HFFs and infected siCPEB1 HFFs. **(b)** Cumulative distribution frequency (CDF) plots of poly(A)-tail length distributions for *UL18*, *UL99*, *UL83-82*-containing and *UL54* HCMV transcripts ($P < 10^{-5}$, $P < 0.00014$, $P < 10^{-20}$ and $P < 0.06$, by one-sided Mann–Whitney U test, respectively). **(c)** CLIP-PCR for RNA targets bound by CPEB1 and FMRP. IP, immunoprecipitation. Error bars, s.e.m. among replicates ($n = 3$ qRT-PCR reactions). Numbers of transcripts (n) are as follows for *UL18*, *UL54*, *UL99* and *UL83-82*, respectively: HCMV, $n = 91, 93, 1,022, 1,034$; CPEB1 KD, $n = 78, 54, 1,341, 1,207$. **(d)** Immunoblot analysis of CPEB1 and viral proteins (IEs, *UL57* and *pp28*) in mock (–) or HCMV (TB40E; +)-infected cells treated with either nontargeting siRNA (siNT) or four different CPEB1-targeting siRNAs (si-02, si-04, si-17 and si-18) at MOIs of 0.5 and 3. β -actin is a loading control. SP, Smartpool (mixture) of four different siRNAs against CPEB1. Uncropped blots are shown in **Supplementary Data Set 10**. Source data for **a–c** are available online.

development^{17,18,24,36}. AS and APA are also perturbed in neuromuscular diseases and cancer^{17,19,37}. However, the scale at which RNA processing events in host transcripts are affected by viral infection, as well as the underlying mechanisms, remains unclear. In our study, despite the wide cellular tropism that distinguishes HCMV, we observed a convergence at the level of RNA processing among different infected cell types. Transcriptome-wide measurements revealed commonly altered AS events in different cell types, thus suggesting shared, cell-type-independent pathways affected by HCMV. AS changes can lead to the production of different proteins either by altering the coding sequence of transcripts or by decreasing protein levels through frameshifts and nonsense-mediated decay, either of which can change the cellular environment in support of viral replication. During infection, the majority of the altered transcripts favored

usage of a proximal poly(A) site, thereby resulting in decreased 3'-UTR lengths that may lead to changes in stability, localization and/or translation of the affected transcripts. 3'-UTR shortening is known to occur in highly proliferative states such as cancer^{37,38}. Furthermore, B cells infected with Epstein–Barr virus demonstrate decreased 3'-UTR lengths for a number of host transcripts³⁹. However, Epstein–Barr virus establishes a latent infection and immortalizes B cells, and the altered host polyadenylation patterns appear to be a consequence of the associated proliferation rather than of the infection itself³⁹. However, during lytic HCMV infection, the cells are not proliferative, thus indicating that global 3'-UTR shortening is not a secondary effect of proliferation.

Identification of RBPs that are responsible for host and viral RNA-processing changes during virus infections will provide key insights

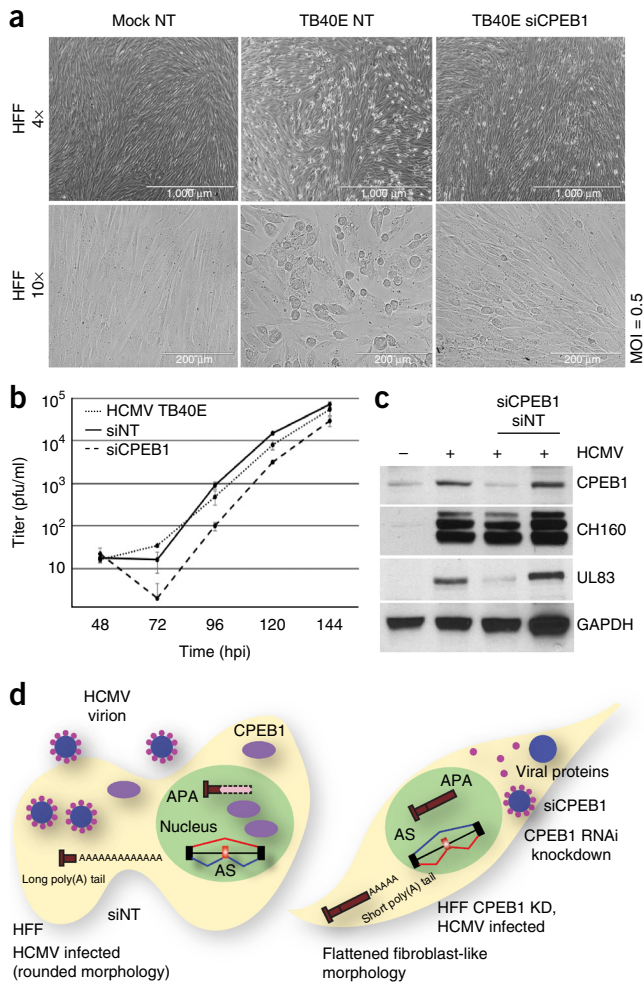


Figure 7 CPEB1 depletion rescues cytopathology and attenuates HCMV infection. **(a)** Phase-contrast images of mock- or HCMV (TB40E)-infected cells treated with either NT or CPEB1 siRNA (siCPEB1) at low (top, 4 \times) and high (bottom, 10 \times) magnifications. The experiment was repeated three times, and representative images are shown. **(b)** Productive HCMV viral titers at different time points, as determined by a plaque assay for TB40E-infected cells (HCMV TB40E), TB40E-infected cells treated with NT (siNT) and TB40E-infected cells treated with CPEB1 siRNA (siCPEB1). $n = 3$ independent plaque measurement assays. Error bars, s.d. among replicates. Pfu, plaque-forming units. **(c)** Immunoblot analysis of CPEB1 and viral proteins (IEs CH160 and UL83) in mock (–) and HCMV (TB40E)-infected cells (MOI 0.5; +) that were left untreated or were treated with NT or CPEB1-targeting siRNA (si17). GAPDH is a loading control. Uncropped blots are shown in **Supplementary Data Set 10**. **(d)** Working model summarizing our findings regarding HCMV infection in the presence (left) and absence (right) of CPEB1. HCMV infection induces CPEB1 expression, which in turn supports certain AS isoforms, shorter 3' UTRs, longer poly(A)-tail lengths and normal productive HCMV titers. In contrast, CPEB1 depletion leads to preservation of normal 3'-UTR lengths and poly(A)-tail lengths, and decreased productive HCMV titers. Source data for **b** are available online.

into mechanisms of viral propagation and transmission and are potential therapeutic targets. We observed consistent upregulation of the RBP CPEB1 in all three primary cell types analyzed. CPEB1 is a well-studied RBP that plays an essential role in early development and neuronal function^{22,32,40}. CPEB1 is known to interact with the splicing factor U2AF65 (ref. 32) and the 3'-end-machinery proteins CPSF-73 and CSTF-64 (ref. 41). CPEB1 binds a consensus sequence

(UUUUUAU), termed the CPE, in introns and 3' UTRs proximal to poly(A) signals^{42–44} and further affects AS⁴¹ and APA in candidate transcripts and minigene reporters³². Our analysis revealed a striking enrichment in CPEs near HCMV-infection-altered 3'-end cleavage sites compared with unaffected 3'-ends. Ectopic expression of CPEB1 in noninfected cells led to a substantial fraction of AS and APA events reminiscent of RNA-processing patterns in HCMV infection. Similarly, CPEB1 depletion during HCMV infection reversed hundreds of RNA processing events and produced a pattern similar to that observed after mock infection. Gene sets altered in APA during infection, CPEB1 overexpression and CPEB1 depletion (during infection) showed enrichment in the categories of extracellular exosome and Golgi apparatus. This finding was particularly salient because HCMV packaging occurs in a membrane-enclosed compartment that contains markers for both the *trans*-Golgi network and endosomes⁴⁵. Furthermore, exosomes and microvesicles (enriched GO terms) can contribute to viral packaging, progression of viral infection, host immune system evasion and allograft rejection^{46–49}.

In the cytoplasm, CPEB1 is linked to the alteration of cytoplasmic polyadenylation and translation of gene transcripts involved in cellular senescence^{50,51}. For example, p53 (*TP53*) mRNA has an abnormally short poly(A) tail and a decreased translational efficiency in CPEB1 KD cells⁵⁰. In our study, transcriptome-wide analysis of poly(A)-tail lengths with TAIL-seq showed an increase in poly(A)-tail lengths of host transcripts during HCMV infection. This phenomenon was in contrast with Kaposi's sarcoma-associated herpesvirus (KSHV) infection, in which the viral protein SOX results in poly(A)-tail extension, nuclear retention and decreased gene expression of host transcripts⁵². We did not observe decreased gene expression of the host transcripts with lengthened poly(A) tails. Furthermore, siRNA-mediated depletion of CPEB1 during HCMV infection not only shortened the median poly(A)-tail lengths to normal levels but also decreased the tail lengths of viral transcripts. GO analysis of host genes whose transcripts had shorter poly(A)-tail lengths after CPEB1 depletion showed an enrichment in the categories of membrane-enclosed lumen and protein localization, thus suggesting viral assembly pathways. Indeed, poly(A)-tail lengths of many members of the small Ras-related protein family (including RABs and small GTPases) were altered, including RAB27A, which is important in HCMV assembly⁵³. We found that HCMV *UL99* and *UL83* contained multicistronic transcripts had shorter poly(A) tails and decreased protein expression after CPEB1 knockdown during infection. Furthermore, CPEB1 directly interacted with viral RNAs containing *UL99* and *UL83*. *UL99*-encoded pp28 is a tegument protein that is essential for final viral envelopment, and a previous report has shown that pp28 knockouts do not produce virions, and infection is attenuated⁵⁴. *UL83* encodes a tegument phosphoprotein that inhibits cellular antiviral response. Notably, both *UL83* and *UL99* gene products (tegument proteins pp65 and pp28, respectively) interact with each other and also with host Golgi and exosomes^{55–57}. Therefore, CPEB1 affects both host and viral components involved in viral assembly.

After HCMV infection, cells became rounded and had bulging nuclei and nuclear inclusions at 48–72 hpi (refs. 58,59). We demonstrated that depletion of CPEB1 not only reversed these cytopathic changes but also decreased the productive HCMV titers by approximately ten-fold at 96 hpi. The titers eventually recovered at later time points, probably because of eventual loss of transiently delivered siRNA and a resurgence of CPEB1. During infection, CPEB1 KD led to a decrease in the *UL99* product pp28. We found that exogenous expression of *UL99* alone by using lentiviruses in the context of CPEB1 depletion was not sufficient to generate HCMV cytopathology.

This result suggests that CPEB1-mediated effects on other HCMV transcripts and proteins may be important in virus infection. Indeed, the late *UL83* product pp65 was also downregulated after CPEB1 depletion during HCMV infection. The immediate early proteins IE 86 and IE 72 were not affected, thus suggesting that viral infection is established, but CPEB1 is required for late stages of virus infection. Because CPEB1 alters host and viral transcripts involved in viral packaging and transport (later stages in infection), our two results of viral packaging dysfunction and inhibition of late infection stages are in strong agreement.

In summary, we demonstrated an unexpected role of CPEB1 induction in productive HCMV infection in HFFs. Our study provides new evidence of the importance of modulating host alternative polyadenylation in host-virus interactions and identifies a new player in these interactions. CPEB1 may not be the only host factor that shapes the host RNA landscape to establish HCMV or other viral infections, and it is likely that other RBPs may be involved. Future work will be important to identify mechanisms of CPEB1 induction, to establish a direct connection between CPEB1 binding and RNA processing with minigene reporters and to understand the roles of other cellular RBPs that affect host and viral RNA landscapes. Finally, this study sheds light on mechanisms of cellular susceptibility to HCMV infection and provides a potential therapeutic target for HCMV. These host mechanisms may extend to other members of the herpesvirus family, and further efforts will be needed to uncover the host RBP-RNA networks dysregulated in DNA virus infections.

METHODS

Methods and any associated references are available in the [online version of the paper](#).

Accession codes. Sequencing data and splicing-sensitive microarray data have been deposited in the Gene Expression Omnibus database under accession number [GSE74250](#).

Note: Any Supplementary Information and Source Data files are available in the [online version of the paper](#).

ACKNOWLEDGMENTS

The authors thank members of the laboratories of G.W.Y. and D.H.S. for critical reading of the manuscript and extend particular acknowledgment to M.T. Lovci (UCSD) for initial assistance with bioinformatics. We thank H. Chang (laboratory of N. Kim, Seoul National University) for help with the Tailseeker algorithm, and S. Azoubel Lima and A. Pasquinelli (UCSD) for sharing their modified TAIL-seq protocol before publication. We especially thank C.S. Morello (UCSD) for assistance with HSV-2 infections, and the laboratory of S.A. Spector (UCSD) for HIV-1-infected materials. This work was partially supported by grants from the National Institutes of Health (HG004659, HG007005 and NS075449 to G.W.Y.) and from the California Institute of Regenerative Medicine (RB3-05219 to G.W.Y. and D.H.S.). T.J.S. and E.C.W. are supported in part by the University of California, San Diego, Genetics Training Program through an institutional training grant from the National Institute of General Medical Sciences, T32 GM008666. E.C.W. is supported as an NSF Graduate Research Fellow. R.B. is supported as a Myotonic Dystrophy Foundation postdoctoral fellow. G.W.Y. is supported as an Alfred P. Sloan Research Fellow.

AUTHOR CONTRIBUTIONS

R.B., T.J.S., D.H.S. and G.W.Y. designed the study and wrote the manuscript; E.C. and J.-P.B. maintained HCMV viral stocks, measured titers and performed HCMV infections; R.B., T.J.S. and E.C. performed siRNA treatments. T.J.S., E.C. and R.B. performed western blots. R.B. performed immunofluorescence and microscopy. T.J.S. and T.J.B. made lentivirus preparations. R.B., T.J.S. and E.C.W. made RNA-seq libraries. R.B., T.J.S., S.C.H., B.A.Y. and S.S. performed bioinformatics analysis. R.B. and T.J.S. performed RT-PCR splicing and APA assays. H.H. and R.B. prepared TAIL-seq libraries, as overseen by S.A. C.G.-B. performed microarray hybridizations. S.C.H., J.P.D. and M.A. performed microarray analysis. R.B., T.J.S. and B.T.R. performed RT-PCR splicing and APA assays. F.R. provided the antisense oligonucleotides.

COMPETING FINANCIAL INTERESTS

The authors declare competing financial interests: details are available in the [online version of the paper](#).

Reprints and permissions information is available online at <http://www.nature.com/reprints/index.html>.

- Staras, S.A. *et al.* Seroprevalence of cytomegalovirus infection in the United States, 1988–1994. *Clin. Infect. Dis.* **43**, 1143–1151 (2006).
- Mocarski, E.S. Betaherpes viral genes and their functions. in *Human Herpesviruses: Biology, Therapy, and Immunoprophylaxis* (eds. Arvin, A. *et al.*), 204–230 (Cambridge University Press, 2007).
- Fortunato, E.A., McElroy, A.K., Sanchez, I. & Spector, D.H. Exploitation of cellular signaling and regulatory pathways by human cytomegalovirus. *Trends Microbiol.* **8**, 111–119 (2000).
- Mocarski, E.S., Shenk, T. & Pass, R.F. Cytomegaloviruses. in *Fields Virology* 5th edn, Vol. 2 (eds. Knipe, D.M. & Howley, P.M.) 2701–2772 (Lippincott Williams & Wilkins, 2007).
- Campbell, L.A. & Rosenfeld, M.E. Infection and atherosclerosis development. *Arch. Med. Res.* **46**, 339–350 (2015).
- DuRose, J.B., Li, J., Chien, S. & Spector, D.H. Infection of vascular endothelial cells with human cytomegalovirus under fluid shear stress reveals preferential entry and spread of virus in flow conditions simulating atheroprone regions of the artery. *J. Virol.* **86**, 13745–13755 (2012).
- Schuessler, A., Walker, D.G. & Khanna, R. Cytomegalovirus as a novel target for immunotherapy of glioblastoma multiforme. *Front. Oncol.* **4**, 275 (2014).
- Horváth, R. *et al.* The possible role of human cytomegalovirus (HCMV) in the origin of atherosclerosis. *J. Clin. Virol.* **16**, 17–24 (2000).
- Fenwick, M.L. & Walker, M.J. Suppression of the synthesis of cellular macromolecules by herpes simplex virus. *J. Gen. Virol.* **41**, 37–51 (1978).
- Sydskis, R.J. & Roizman, B. Polysomes and protein synthesis in cells infected with a DNA virus. *Science* **153**, 76–78 (1966).
- Kwong, A.D. & Frenkel, N. Herpes simplex virus-infected cells contain a function(s) that destabilizes both host and viral mRNAs. *Proc. Natl. Acad. Sci. USA* **84**, 1926–1930 (1987).
- Hertel, L. & Mocarski, E.S. Global analysis of host cell gene expression late during cytomegalovirus infection reveals extensive dysregulation of cell cycle gene expression and induction of pseudomitosis independent of US28 function. *J. Virol.* **78**, 11988–12011 (2004).
- Gatherer, D. *et al.* High-resolution human cytomegalovirus transcriptome. *Proc. Natl. Acad. Sci. USA* **108**, 19755–19760 (2011).
- Stern-Ginossar, N. *et al.* Decoding human cytomegalovirus. *Science* **338**, 1088–1093 (2012).
- Poulos, M.G., Batra, R., Charizanis, K. & Swanson, M.S. Developments in RNA splicing and disease. *Cold Spring Harb. Perspect. Biol.* **3**, a000778 (2011).
- Ulitsky, I. *et al.* Extensive alternative polyadenylation during zebrafish development. *Genome Res.* **22**, 2054–2066 (2012).
- Batra, R. *et al.* Loss of MBNL leads to disruption of developmentally regulated alternative polyadenylation in RNA-mediated disease. *Mol. Cell* **56**, 311–322 (2014).
- Scotti, M.M. & Swanson, M.S. RNA mis-splicing in disease. *Nat. Rev. Genet.* **17**, 19–32 (2016).
- Charizanis, K. *et al.* Muscleblind-like 2-mediated alternative splicing in the developing brain and dysregulation in myotonic dystrophy. *Neuron* **75**, 437–450 (2012).
- Jenal, M. *et al.* The poly(A)-binding protein nuclear 1 suppresses alternative cleavage and polyadenylation sites. *Cell* **149**, 538–553 (2012).
- de Klerk, E. *et al.* Poly(A) binding protein nuclear 1 levels affect alternative polyadenylation. *Nucleic Acids Res.* **40**, 9089–9101 (2012).
- Richter, J.D. CPEB: a life in translation. *Trends Biochem. Sci.* **32**, 279–285 (2007).
- Scorilas, A. Polyadenylate polymerase (PAP) and 3' end pre-mRNA processing: function, assays, and association with disease. *Crit. Rev. Clin. Lab. Sci.* **39**, 193–224 (2002).
- Subtelny, A.O., Eichhorn, S.W., Chen, G.R., Sive, H. & Bartel, D.P. Poly(A)-tail profiling reveals an embryonic switch in translational control. *Nature* **508**, 66–71 (2014).
- Chang, H., Lim, J., Ha, M. & Kim, V.N. TAIL-seq: genome-wide determination of poly(A) tail length and 3' end modifications. *Mol. Cell* **53**, 1044–1052 (2014).
- Licatalosi, D.D. *et al.* HITS-CLIP yields genome-wide insights into brain alternative RNA processing. *Nature* **456**, 464–469 (2008).
- Katz, Y., Wang, E.T., Airoidi, E.M. & Burge, C.B. Analysis and design of RNA sequencing experiments for identifying isoform regulation. *Nat. Methods* **7**, 1009–1015 (2010).
- Huelga, S.C. *et al.* Integrative genome-wide analysis reveals cooperative regulation of alternative splicing by hnRNP proteins. *Cell Rep.* **1**, 167–178 (2012).
- Gehman, L.T. *et al.* The splicing regulator Rbfox1 (A2BP1) controls neuronal excitation in the mammalian brain. *Nat. Genet.* **43**, 706–711 (2011).
- Belzile, J.P., Stark, T.J., Yeo, G.W. & Spector, D.H. Human cytomegalovirus infection of human embryonic stem cell-derived primitive neural stem cells is restricted at several steps but leads to the persistence of viral DNA. *J. Virol.* **88**, 4021–4039 (2014).



31. Luo, W. *et al.* The conserved intronic cleavage and polyadenylation site of CstF-77 gene imparts control of 3' end processing activity through feedback autoregulation and by U1 snRNP. *PLoS Genet.* **9**, e1003613 (2013).
32. Bava, F.A. *et al.* CPEB1 coordinates alternative 3'-UTR formation with translational regulation. *Nature* **495**, 121–125 (2013).
33. Huang, W., Sherman, B.T. & Lempicki, R.A. Systematic and integrative analysis of large gene lists using DAVID bioinformatics resources. *Nat. Protoc.* **4**, 44–57 (2009).
34. Szklarczyk, D. *et al.* STRING v10: protein-protein interaction networks, integrated over the tree of life. *Nucleic Acids Res.* **43**, D447–D452 (2015).
35. Kim, Y. *et al.* Human cytomegalovirus UL18 utilizes US6 for evading the NK and T-cell responses. *PLoS Pathog.* **4**, e1000123 (2008).
36. Batra, R., Manchanda, M. & Swanson, M.S. Global insights into alternative polyadenylation regulation. *RNA Biol.* **12**, 597–602 (2015).
37. Mayr, C. & Bartel, D.P. Widespread shortening of 3'UTRs by alternative cleavage and polyadenylation activates oncogenes in cancer cells. *Cell* **138**, 673–684 (2009).
38. Sandberg, R., Neilson, J.R., Sarma, A., Sharp, P.A. & Burge, C.B. Proliferating cells express mRNAs with shortened 3' untranslated regions and fewer microRNA target sites. *Science* **320**, 1643–1647 (2008).
39. Homa, N.J. *et al.* Epstein-Barr virus induces global changes in cellular mRNA isoform usage that are important for the maintenance of latency. *J. Virol.* **87**, 12291–12301 (2013).
40. Weill, L., Belloc, E., Bava, F.A. & Méndez, R. Translational control by changes in poly(A) tail length: recycling mRNAs. *Nat. Struct. Mol. Biol.* **19**, 577–585 (2012).
41. Lin, C.L., Evans, V., Shen, S., Xing, Y. & Richter, J.D. The nuclear experience of CPEB: implications for RNA processing and translational control. *RNA* **16**, 338–348 (2010).
42. Mendez, R. *et al.* Phosphorylation of CPE binding factor by Eg2 regulates translation of c-mos mRNA. *Nature* **404**, 302–307 (2000).
43. Mendez, R. & Richter, J.D. Translational control by CPEB: a means to the end. *Nat. Rev. Mol. Cell Biol.* **2**, 521–529 (2001).
44. Fox, C.A., Sheets, M.D. & Wickens, M.P. Poly(A) addition during maturation of frog oocytes: distinct nuclear and cytoplasmic activities and regulation by the sequence UUUUUUU. *Genes Dev.* **3**, 2151–2162 (1989).
45. Cepeda, V., Esteban, M. & Fraile-Ramos, A. Human cytomegalovirus final envelopment on membranes containing both trans-Golgi network and endosomal markers. *Cell. Microbiol.* **12**, 386–404 (2010).
46. Walker, J.D., Maier, C.L. & Pober, J.S. Cytomegalovirus-infected human endothelial cells can stimulate allogeneic CD4+ memory T cells by releasing antigenic exosomes. *J. Immunol.* **182**, 1548–1559 (2009).
47. Wurdinger, T. *et al.* Extracellular vesicles and their convergence with viral pathways. *Adv. Virol.* **2012**, 767694 (2012).
48. Plazolles, N. *et al.* Pivotal advance: the promotion of soluble DC-SIGN release by inflammatory signals and its enhancement of cytomegalovirus-mediated cis-infection of myeloid dendritic cells. *J. Leukoc. Biol.* **89**, 329–342 (2011).
49. Schorey, J.S., Cheng, Y., Singh, P.P. & Smith, V.L. Exosomes and other extracellular vesicles in host-pathogen interactions. *EMBO Rep.* **16**, 24–43 (2015).
50. Burns, D.M. & Richter, J.D. CPEB regulation of human cellular senescence, energy metabolism, and p53 mRNA translation. *Genes Dev.* **22**, 3449–3460 (2008).
51. Groppo, R. & Richter, J.D. CPEB control of NF- κ B nuclear localization and interleukin-6 production mediates cellular senescence. *Mol. Cell. Biol.* **31**, 2707–2714 (2011).
52. Lee, Y.J. & Glaunsinger, B.A. Aberrant herpesvirus-induced polyadenylation correlates with cellular messenger RNA destruction. *PLoS Biol.* **7**, e1000107 (2009).
53. Fraile-Ramos, A., Cepeda, V., Elstak, E. & van der Sluijs, P. Rab27a is required for human cytomegalovirus assembly. *PLoS One* **5**, e15318 (2010).
54. Silva, M.C., Yu, Q.C., Enquist, L. & Shenk, T. Human cytomegalovirus UL99-encoded pp28 is required for the cytoplasmic envelopment of tegument-associated capsids. *J. Virol.* **77**, 10594–10605 (2003).
55. Sanchez, V., Sztul, E. & Britt, W.J. Human cytomegalovirus pp28 (UL99) localizes to a cytoplasmic compartment which overlaps the endoplasmic reticulum-golgi-intermediate compartment. *J. Virol.* **74**, 3842–3851 (2000).
56. Tomtishen, J.P. III. Human cytomegalovirus tegument proteins (pp65, pp71, pp150, pp28). *J. Virol.* **9**, 22 (2012).
57. Liu, S.T. *et al.* Synaptic vesicle-like lipidome of human cytomegalovirus virions reveals a role for SNARE machinery in virion egress. *Proc. Natl. Acad. Sci. USA* **108**, 12869–12874 (2011).
58. Albrecht, T., Cavallo, T., Cole, N.L. & Graves, K. Cytomegalovirus: development and progression of cytopathic effects in human cell culture. *Lab. Invest.* **42**, 1–7 (1980).
59. Cavallo, T., Graves, K., Cole, N.L. & Albrecht, T. Cytomegalovirus: an ultrastructural study of the morphogenesis of nuclear inclusions in human cell culture. *J. Gen. Virol.* **56**, 97–104 (1981).



ONLINE METHODS

Cell types. Neural precursor cells (NPCs) were derived from H9 and HUES9 human ES cells. We used primary human foreskin fibroblasts (HFFs) as in ref. 30, and ECs as ref. 6. Cells were routinely tested for mycoplasma contamination with a MycoAlert mycoplasma test kit (Lonza) and were found negative for mycoplasma.

Virus infections. All TB40E HCMV infections were performed as previously described³⁰. HUES9-derived NPCs were primarily used in this study, and H9-derived cells were used in extended follow-up comparisons (**Supplementary Fig. 3d,e**). Towne HCMV infections (RT-PCR comparisons shown in **Fig. 1c**) were conducted at an MOI of 3. For IFN- γ treatment, 500 U or 25 ng/ml of recombinant IFN- γ (Abcam ab9659) in MEM plus 10% FBS was used for the treatment of HFFs. For UV treatment, HCMV was exposed to a dose of 400 mJ/cm² of UV light in a Stratalink cross-linker (Stratagene). HSV-2 infections were performed in HFFs of strain G at an MOI of 10. For HSV-2, after an initial 30-min adsorption period at 4 °C, mock-infected and infected cells were incubated at 37 °C and harvested at 2 or 8 hpi. All HCMV and HSV-2 materials were collected at the time of harvest by trypsinization, briefly pelleted and snap frozen before subsequent analysis. HIV-1 infections of T-cell cultures were performed as described⁶⁰ and harvested directly into TRIzol (Life Technologies) 5 d after infection.

RNA-seq library preparation and data processing. Total RNA was isolated with TRIzol reagent, per the manufacturer's protocol (Life Technologies). For all the HCMV TB40E-infection and mock-infection conditions, we prepared strand-specific libraries with the dUTP method⁶¹ with adaptations previously described in detail²⁸. For the TB40E and mock-infected HFFs and ECs, adaptor-containing oligo(dT) was included during first-strand cDNA synthesis (cDNA Cloning Primer, ReadyMade Primers, Integrated DNA Technologies). Libraries for the comparative analysis of mock, HCMV, siCPEB1 and CPEB1 OE samples were prepared with Illumina TruSeq poly(A) mRNA Sample Preparation reagents. All samples were sequenced on an Illumina HiSeq platform. Each sample was barcoded, multiplexed and run together. Cluster 3.0 and Java Treeview were used in combination to perform and visualize results from hierarchical gene-expression clustering results. Libraries for analysis of HSV-2 infections were prepared with Illumina TruSeq Stranded mRNA Sample Preparation reagents. HSV-2 samples were multiplexed and run together.

Analysis of HCMV gene expression. For HCMV mRNA abundance measurements, we used the newly available TB40E genome sequence (GenBank [KF297339.1](https://www.ncbi.nlm.nih.gov/nuccore/KF297339.1), strain 'Lisa') for mapping and analysis of coverage of GenBank-listed HCMV ORF annotations. Data processing was also performed with the HCMV Merlin reference to facilitate comparisons to previous studies by Gatherer *et al.* and Stern-Ginossar *et al.*^{13,14}.

Analysis of human alternative splicing and polyadenylation. Splicing-sensitive microarray analysis was performed as previously described²⁸. RT-PCR splicing assays were performed with the equivalent of 50 ng of oligo(dT)-primed cDNA (reverse transcription performed with Superscript III, Life Technologies) and 35 cycles of PCR amplification. For AS analysis of RNA-seq data, we used Olego and the Qantas software suite as previously described^{19,62}. Tandem UTR isoform analysis was performed with the MISO algorithm v0.5.2 with default settings²⁷, except for use of custom 3'-UTR-isoform annotations. We used a Bayes-factor threshold of 10,000 and difference values ($\Delta\psi$) with an absolute value of at least 0.03 (although the cutoff selected for this latter value was low, we found significant degrees of UTR shift from this value upward, when it was used in combination with the high Bayes factor for the HCMV samples). To generate the custom annotations, we downloaded all Ensembl-defined human 3'-UTR regions (<http://www.ensembl.org/>, release 75) and flattened them with the mergeBed function from Bedtools v2.16.2 (to define 3'-UTR starts). Collapsed UTR regions with more than one cleavage site detected by RNA-seq were considered, with a minimum threshold of five reads required to constitute a poly(A) site. These cleavage-defining reads were based on human-mapped poly(A)₆⁺-containing RNA-seq reads (with filtering performed for genomic regions with A tracts). Finally, the two termination sites with the highest coverage were selected to define putative proximal and distal alternative ends of the 3' UTRs. We generated one index on the basis of

poly(A) reads from the infected NPCs and generated another that was based on a composite of infected HFF and EC poly(A) reads (neuronal versus non-neuronal was sufficient for this analysis, and we had obtained a sequencing depth of 1.5× to 2× in the NPC samples versus the HFF and EC libraries). Indexed annotations were generated separately for the HSV-2 condition, again on the basis of the samples' own poly(A) RNA-seq reads. qRT-PCR analysis of alternative 3'-UTR isoforms was performed as previously described¹⁶. 1 μ g of total RNA was first DNase treated, and only oligo(dT) was used for cDNA synthesis (generated with Superscript III, Life Technologies). All primer sequences for RT-PCR and qPCR reactions are provided in **Supplementary Data Set 11**.

Western blot analysis. Whole cell lysates were prepared from cell pellets that had been stored at -80 °C, with RIPA lysis buffer, on ice. After brief sonication, lysates were clarified by 12,000g centrifugation for 10–15 min. Samples were loaded according to total protein content, as determined by BCA assessment (Thermo Pierce), and within each cell type the amounts were normalized to the first mock-infected sample (corresponding to ~100,000 cells total per lane). Antibodies to the following proteins were used at the indicated dilutions: CSTF-64 (A301-092A), CSTF-77 (A301-096A) and CFI_m-68 (A301-356A) from Bethyl Laboratories, 1:2,000; CPEB1 (13583) from Cell Signaling Technologies, 1:1,000; β -actin (clone AC-15, A1978) from Sigma-Aldrich, 1:10,000; mouse IE (CH160) from Virusys, 1:5,000; mouse UL57 from Virusys, 1:1,000; mouse UL99 (pp28) from Virusys, 1:1,000; and mouse UL83 (pp65) from Virusys, 1:5,000. Validation information is provided on the manufacturers' websites.

Lentiviral vector production and transduction. The human CPEB1 open reading frame was PCR amplified from HFF cDNA with the following primers: forward, GCCCGCTGCAAAAATAGTG; reverse, TCAGCAAGTGCAAAGGTGAC. The PCR product was first cloned into the Topo-TA vector pCR2.1 (Life Technologies). CMV-turboGFP from pGIPZ (Open Biosystems) was replaced with the CMV promoter from pCDNA3.1- (Life Technologies), and the cloned CPEB1 was inserted at the SpeI and NotI restriction sites. CPEB1, UL99 and control GFP lentiviruses were generated in 293T cells with PEI transfection reagent, in 10-cm format with 10⁷ cells per dish, with the second-generation packaging constructs psPAX2 and pMD2.G. Supernatants were harvested at 60 h post-transfection and run through a 0.22- μ m filter. Freshly seeded HFFs were transduced at an MOI of 0.5 to 1, without polybrene or additional reagents. Puromycin selection was initiated in the transduced HFFs at 48 h, and cells were harvested after 3 d of drug selection.

TAIL-seq. TAIL-seq was performed as previously described by Chang *et al.*²⁵, with minor modifications. Briefly, total RNA was extracted from cells with TRIzol reagent (Life Technologies) according to the manufacturer's protocol. The RNA was ligated to 3' 'splint' oligonucleotides (NNNGTCAGTTTTTTTTT) to enrich for polyadenylated transcripts and was partially digested with RNase T1 (Ambion). The fragmented RNAs were pulled down with Dynabeads M-280 streptavidin (Invitrogen) magnetic beads, phosphorylated on bead with a T4-PNK reaction kit (NEB), eluted with 2× RNA loading dye (with 95% formamide), run on a 6% polyacrylamide urea gel (NuPage), stained with SYBR gold (Thermo) and gel purified in the range of 250–750 nt. The purified RNAs were ligated to 5' adaptors (Illumina TruSeq small RNA kit), reverse transcribed with Superscript III (Invitrogen) and amplified by PCR with Phusion DNA polymerase (Thermo) and Illumina TruSeq small RNA universal forward and indexed (barcode) reverse primer(s). The library was purified with AMPureXP beads (Agilent) and sequenced on an Illumina MiSeq instrument (51 × 251-bp paired-end runs) with 10% PhiX control library (Illumina) and 1% spike-in mixture consisting of known poly(A)-containing DNAs²⁵. All adapters and primers were synthesized by IDT.

Antisense oligonucleotide (ASO) transfections. 5 × 10⁴ HFFs were seeded per well of a 12-well plate. For each ASO, 2 μ l of 200- μ M stock ASO was mixed with 100 μ l of OptiMEM (Gibco) and 3 μ l of RNAiMax (Life Sciences), incubated for 30 min at room temperature and added to the respective well. HCMV infection was initiated 24 h after ASO transfection.

Statistical methods. The qPCRs were compared in a pairwise analysis, and *P* values were calculated with Student's *t* test among technical replicates. The

error bars are reported as s.d. or standard error of the technical replicates, as mentioned in the respective figure legends. Genome-wide APA analysis was performed with the MISO algorithm v0.5.2, and Bayes factor and $\Delta\Psi$ values were calculated. The Bayes factor represents the weight of the evidence of the data in favor of versus not in favor of differential expression, as described by Katz *et al.*²⁷. We used a Bayes-factor threshold of 10,000 and difference values ($\Delta\Psi$) with an absolute value of at least 0.03. A Bayes factor of 10,000 indicates that an APA switch is 10,000 times more likely to occur than not. For gene expression, reads were trimmed for adaptor sequences or low-quality bases and then mapped to both the human genome (hg19 build) and the HCMV Merlin genome (GenBank [AY446894.2](#)) with GSNAP. Additional filtering of reads that mapped to repetitive elements was also performed. Gene-expression values (in RPKM⁶³) were calculated within each sample, and Z-score analysis was implemented to identify significant differences in expression, as previously described⁶⁴. For AS analysis, we followed the procedure described in Charizanis *et al.*¹⁹. For each pair of reads that spanned one or more exons (up to three, which is sufficient in practice given the fragment size), all possible isoforms (paths) between the anchored ends were found, and the probability of each isoform being the actual origin of the paired-end reads was estimated. Each inferred fragment was assigned a probability score. This junction inference step substantially increased the effective number of fragments supporting exon junctions, especially for cassette exons, and increased the statistical power in detecting splicing changes. The weighted number of exon or exon-junction fragments uniquely supporting the inclusion or skipping isoform of each cassette exon was counted, and Fisher's exact test was used to evaluate the statistical significance of splicing changes with both exon and exon-junction fragments and was then followed by Benjamini–Hochberg multiple hypothesis testing correction to estimate the FDR. Differential splicing

events were identified by requiring FDR <0.05 and $|\Delta I| \geq 0.1$. For TAIL-seq data analysis, image files were downloaded from the MiSeq instrument and run on tailseeker2 (ref. 25) to determine accurate poly(A)-tail lengths, thus yielding paired fastq files corresponding to the 5' (R5) and 3' (R3 poly(A) tail) ends of each read. Reads were aligned against the human genome (hg19) and viral genomes (human_herpesvirus_5_strain_Merlin) with STAR under default parameters. Features were assigned with Subread with gencode v19 annotations and with human_herpesvirus_5_strain_Merlin features, and filtered to obtain only the uniquely mapped protein-coding genes. For analysis of virally mapped reads, all genes were counted. Reads with tails with lengths measuring 0 were removed. For genes with at least 20 mapped reads, median lengths were measured, and the global distributions of these lengths were compared with the Kolmogorov–Smirnov test. Individual tail-length distributions were compared among samples with the Mann–Whitney *U* test, with a *P*-value cutoff of 0.025.

60. Noraz, N., Gozlan, J., Corbeil, J., Brunner, T. & Spector, S.A. HIV-induced apoptosis of activated primary CD4⁺ T lymphocytes is not mediated by Fas-Fas ligand. *AIDS* **11**, 1671–1680 (1997).
61. Parkhomchuk, D. *et al.* Transcriptome analysis by strand-specific sequencing of complementary DNA. *Nucleic Acids Res.* **37**, e123 (2009).
62. Wu, J., Anczuków, O., Krainer, A.R., Zhang, M.Q. & Zhang, C. OLego: fast and sensitive mapping of spliced mRNA-Seq reads using small seeds. *Nucleic Acids Res.* **41**, 5149–5163 (2013).
63. Mortazavi, A., Williams, B.A., McCue, K., Schaeffer, L. & Wold, B. Mapping and quantifying mammalian transcriptomes by RNA-Seq. *Nat. Methods* **5**, 621–628 (2008).
64. Polymenidou, M. *et al.* Long pre-mRNA depletion and RNA missplicing contribute to neuronal vulnerability from loss of TDP-43. *Nat. Neurosci.* **14**, 459–468 (2011).